



OPEN ACCESS

EDITED BY

Lingjun Kong,
Guangzhou University, China

REVIEWED BY

Titus Egboisiuba,
Chukwuemeka Odumegwu Ojukwu
University, Nigeria
Koorosh Gharehbaghi,
RMIT University, Australia

*CORRESPONDENCE

Martin J. Taylor,
✉ martin.taylor@hull.ac.uk
Surinder K. Mehta,
✉ skmehta@pu.ac.in

RECEIVED 17 May 2023

ACCEPTED 10 July 2023

PUBLISHED 19 July 2023

CITATION

Priyanka, Vashisht D, Taylor MJ and
Mehta SK (2023), Evaluating the pre-
treatment protocol required to produce
an effective carbonized waste adsorbent
for organic pollution control.
Front. Environ. Sci. 11:1224388.
doi: 10.3389/fenvs.2023.1224388

COPYRIGHT

© 2023 Priyanka, Vashisht, Taylor and
Mehta. This is an open-access article
distributed under the terms of the
[Creative Commons Attribution License
\(CC BY\)](https://creativecommons.org/licenses/by/4.0/). The use, distribution or
reproduction in other forums is
permitted, provided the original author(s)
and the copyright owner(s) are credited
and that the original publication in this
journal is cited, in accordance with
accepted academic practice. No use,
distribution or reproduction is permitted
which does not comply with these terms.

Evaluating the pre-treatment protocol required to produce an effective carbonized waste adsorbent for organic pollution control

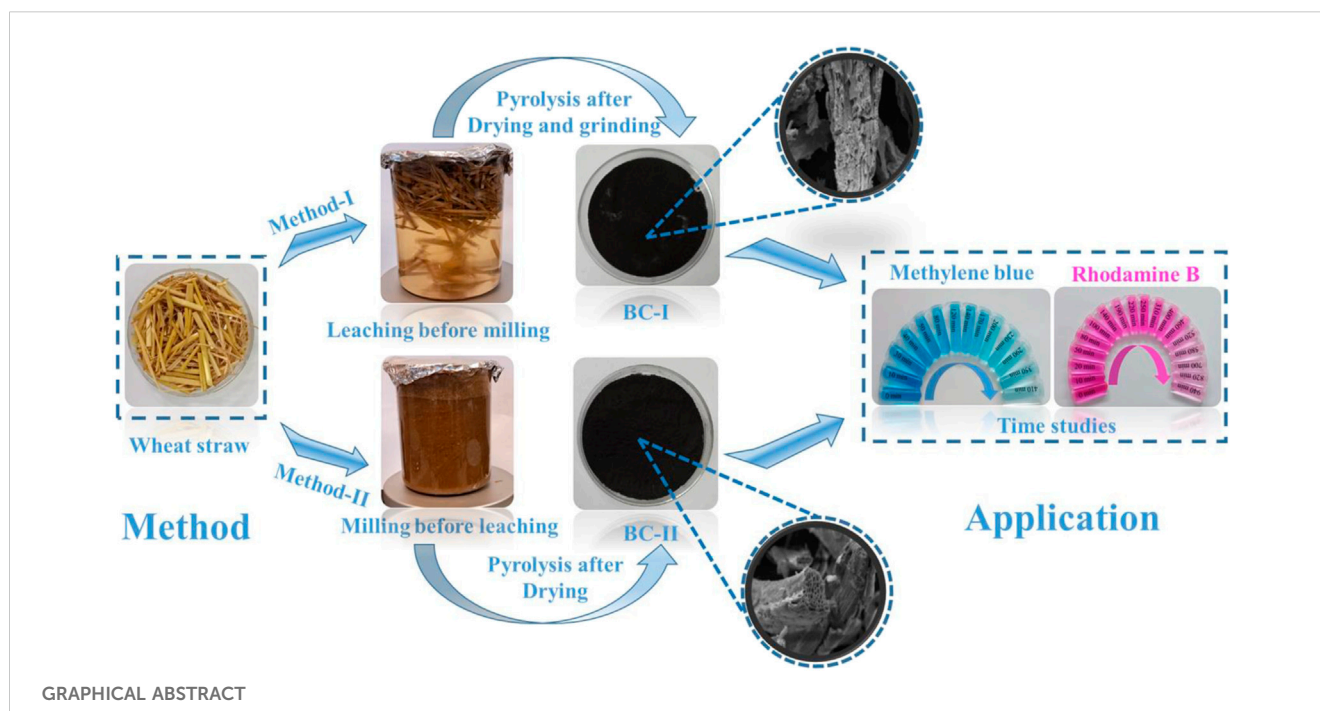
Priyanka^{1,2}, Devika Vashisht¹, Martin J. Taylor^{2*} and
Surinder K. Mehta^{1,3*}

¹Department of Chemistry and Centre for Advanced Studies in Chemistry, Panjab University, Chandigarh, India, ²School of Engineering, Chemical Engineering, University of Hull, Hull, United Kingdom, ³Department of Chemistry, University of Ladakh, Kargil, India

With the goal of fostering the circular economy, the present work was devised to minimize and manage agricultural waste by transforming it into biochar; a versatile dye removal adsorbent. Waterways across the globe are frequently fouled and contaminated with organic materials, especially via unregulated industrial effluents, producing toxic water supplies. Rhodamine B (RhB) and Methylene blue (MB) dyes were used as model organic pollutants in water. The contaminants were then readily extracted from environmental samples using sustainable wheat straw derived biochars. These materials were utilized in an effort to link the circular economy directly to environmental protection, reducing organic contamination by using a low carbon solution. Herein, two methods were adopted to refine a low temperature carbonized material, dependent on initial pre-treatment; leaching followed by milling (method-I) and milling followed by leaching (method-II). Scanning Electron Microscopy (SEM), nitrogen physisorption, proximate and ultimate analysis and Attenuated Total Reflectance-Fourier Transform Infrared Spectroscopy (ATR-FTIR) were used to examine the properties of the synthesized materials. It was found that by altering the process of initial waste pre-treatment, an increase in available surface area ($6.284 \text{ m}^2\text{g}^{-1}$ – $20.754 \text{ m}^2\text{g}^{-1}$) and pore structure can be found post feedstock pyrolysis. Additionally, FTIR of the biochar post extraction supported the adsorption process of both dyes, demonstrating a change in dye-adsorbent bonding, depending on the initial waste pre-treatment for the biochar. In batch mode, several operating parameters including pH, concentration, duration, and dose were optimized. Kinetics and adsorption isotherm studies for biochar synthesized by method-II pre-treatment (BC-II) revealed that the system follows Pseudo-first-order kinetics and Freundlich adsorption isotherm model with the relative R^2 of 0.9989 and 0.9880 for RhB, comparing with 0.9933 and 0.9932 for MB. The optimal produced biochar, BC-II effectively removed 91.06% of RhB from solution at pH 4 and 92.43% for MB at pH 8. This study brings forth a solution to enhance waste management by creating a circular scenario and alleviate environmental contamination by utilizing wheat straw as a biochar adsorbent, produced under controlled and low temperature conditions.

KEYWORDS

biochar, methylene blue, rhodamine B, adsorption, environmental protection, water pollution



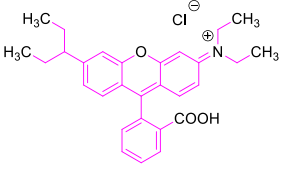
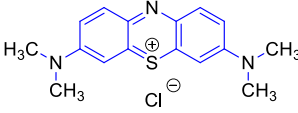
1 Introduction

The backbone of a strong economy is a reliable supply of clean drinking water, but this issue is chronically underemphasized, globally. Concern over having clean drinking water is increasing among a section of the global population (Jury and Vaux, 2005). Water supplies are becoming rapidly contaminated as a result of anthropogenic activity and the rapidly expanding population (Palansooriya et al, 2020). “Clean Water and Sanitation” is the sixth Sustainable Development Goal (SDG), however, according to the World Health Organization (WHO), 2.1 billion people still lack access to properly regulated drinking water. In 2017, statistics from the WHO and the United Nations International Children’s Emergency Fund (UNICEF) mention that surface water sources for 159 million people still serve as the sole supply of drinking water (Kumar et al, 2022). The arduous issue associated with it is that surface water is contaminated with both inorganic and organic pollutants, these include anionic, cationic, and azo dyes (Chen et al, 2022). At an industrial scale across the planet, different materials, including paper, leather, and textiles, are frequently coloured with dyes, and these colours easily degrade in water (Wang et al, 2016). Thus, more than 10%–15% of the 10,000 different types of hazardous organic dyes discharged into aquatic systems come from industrial production processes (Anfar et al, 2019). Thiazine dyes like Methylene Blue (MB) can cause burns, eye damage, mental confusion, nausea and excessive perspiration when it is present in wastewater (Moharm et al, 2022). Moreover, a xanthine dye such as Rhodamine B (RhB) is known to be toxic, carcinogenic and found to have adverse consequences on peoples’ health, especially when ingested (Li et al, 2022).

A high-capacity approach must be utilized to effectively and efficiently extract/decompose these dyes from wastewater

(Veeramalai et al, 2022). Numerous techniques have been documented for the removal of dyes from water supplies. Cationic dyes such as MB, RhB, and Rhodamine 6G (RB6G) have been found to rapidly adsorb to dodecahydro-closo-dodecaborate anion organic polymers (Zhao et al., 2018). On irradiating with UV light, Somashekharappa et al, synthesized nanoparticles and nanotubes by using potassium hexatitanate via a hydrothermal method that was found to directly decompose MB and RhB (Kenchappa Somashekharappa and Lokesh, 2021). When subjected to a 125 W highly pressurized mercury lamp (365 nm, 20 mW/cm²) and a tungsten silicic acid/zeolite composite, methyl orange has been found to photodegrade (Leal Marchena et al, 2016). Organic dyes can also be eliminated via nanofiber aminated polyacrylonitrile membranes (Zhao et al, 2022). Additionally, methyl orange has been found to be broken down by a C₆₀/SiO₂ composite when exposed to visible light (Wakimoto et al, 2015). For the removal of organic dyes from water bodies, filter papers treated with carboxymethyl have also been employed to remove both the soluble dye and inorganic sediment (Xiao et al, 2021). Sustainable derived dye removal technologies are not new, many others have been reported in the literature such as Egbosiuba et al created biochar from empty fruit bunches (Egbosiuba et al, 2020). Adekola et al produced a plantain peel biochar at 500°C, with a removal efficiency of 54.78% for RhB that was adsorbable at pH 7 (Adekola et al, 2019). In another study by Yu et al, biomass produced from baker’s yeast was used as an adsorbent for the removal of RhB and MB dyes, this was also found to be regeneratable using acidic TiO₂ hydrosol (xia et al, 2009). In a study by Tehrani et al, MB and RhB, both of which are thought to be toxic and possibly carcinogenic, were removed simultaneously from an aqueous solution using the metal organic framework MIL-68, which has metal sites for aluminium ions [i.e., MIL-68(Al)] (Saghanejhad Tehrani and Zare-Dorabei, 2016). Toledo and

TABLE 1 Physical and chemical properties of RhB and MB dyes.

Dye	IUPAC name	Chemical formula	Chemical structure	Mol. Wt. (g mol ⁻¹)	λ _{max} (nm)
RhB	9-(2-Carboxyphenyl)-6-(diethylamino)-N,N-diethyl-3H-xanthen-3-iminium chloride	C ₂₈ H ₃₁ ClN ₂ O ₃		479.02	554
MB	[7-(dimethylamino) phenothiazin-3-ylidene]-dimethylazanium; chloride	C ₆ H ₁₈ N ₃ ClS		319.90	664

co-workers studied Tryptophan (Trp) decorated hydroxypropyl methylcellulose (HPMC) cryogels and their influence on the adsorption of MB and RhB (Toledo et al, 2020). Onu and others synthesize green nickel oxide nanoparticles using fresh guava leaves for the adsorption of MB dye and Pb (II) ions (Chukwu Onu et al, 2023). However, a study into the methodology behind biochar development, specifically initial waste pre-treatment procedure is missing from the literature. Additionally, although low temperature pyrolysis routes have been followed, there is limited information pertaining to the use of materials being used at the onset of pyrolysis, leading to the production energy efficient lignin-based materials.

As an effective and popular adsorbent, carbonaceous materials in the form of activated carbons have been developed and applied (Greenwald et al, 2015; Yin et al, 2022). However, the expense of utilizing activated carbons to remove dyes impede their widespread application in the treatment of textile effluents (Wang et al, 2016). To effectively eliminate dyes from contaminated water, a low-cost, sustainable and energy efficient solution must be developed to allow for large scale remediation activities.

India is a world leader in agriculture for crops, second only to China (Singh, 2016). Over 500 million tons of agricultural waste is produced each year as a result of such farming activities, according to the Ministry of New and Renewable Energy (MNRE). One of India's major crops is wheat straw, the conventional method of handling wheat straw waste, after processing involves burning it in the field which has significantly tainted the air (Li et al, 2007). Many strategies have been developed to recycle waste, such as wheat straw by creating biochars, these entities have the potential to be used to treat wastewater, sequester carbon dioxide, and remediate soil because of their often high surface area and micro porosity (Manyà, 2012; Wang et al, 2015). Biochar is produced from lignocellulosic biomass waste as the major product from slow pyrolysis (Yaashikaa et al, 2020a; Eltaweil et al, 2022). In addition to having a high carbon content and high cation exchange capacity, biochar can also possess an alkaline nature, depending on its parent feedstock (Rizwan et al, 2016). Various forms of biomass, industrial waste, and agricultural wastes such as coconut husks, rice straw and corncobs are routinely pyrolysed slowly to produce biochar for commercial applications such as domestic water filters (Ahmed et al, 2016). The type of biomass,

heating rate, pyrolysis process, and residence time all have a substantial impact on the characteristics of the produced solid material (Zhang et al, 2017).

In the current work, two materials were created and denoted as BC-I and BC-II, their naming is based around two pre-treatment regimes investigated: (I) leaching in deionised water, drying followed by milling (physicochemical-physical) and (II) milling followed by leaching in deionised water, and then drying (physical-physicochemical) (Taylor et al, 2019). The feedstocks were then carbonised at the lower end of the pyrolysis temperature range (400°C). The resulting chars once cleaned were characterised using nitrogen physisorption (surface area and porosity measurements), Attenuated Total Reflectance-Fourier Transform Infrared Spectroscopy (ATR-FTIR), thermogravimetric analysis, elemental analysis (CHN), and Scanning Electron Microscopy. Rhodamine B (RhB) and Methylene Blue (MB) have been chosen to serve as model dyes and Table 1 lists their characteristics. These dyes were chosen due to their inability to naturally degrade in water, interacting with biodiversity and damaging aquatic ecosystems (Waghchaure et al, 2022). For the adsorption of RhB and MB by BC-I and BC-II, the effects of pH, duration studies, amount of adsorbent, concentration studies, adsorption kinetics, and adsorption isotherms were examined in this study. The innovative aspect of the research is to convert waste materials into efficient and ecologically friendly adsorbent materials from a more environmentally favorable and carbon neutral source, wheat straw.

2 Experimental section

2.1 Reagents

Locally sourced wheat straw from the Mansa district of Punjab, India was collected. Sodium hydroxide pellets (minimum assay 97.0%) were purchased from Thermo Fisher Scientific India Pvt. Ltd. and hydrochloric acid (extrapure) was from FINAR. Ethanol (absolute) and acetone (99.8%) were from Changshu Hongsheng Fine Chemical Co., Ltd. Rhodamine B (≥95%) was purchased from Sigma Aldrich, India. Methylene Blue (>90%) was purchased from CDH (Central Drug House). In this experiment, all solutions were

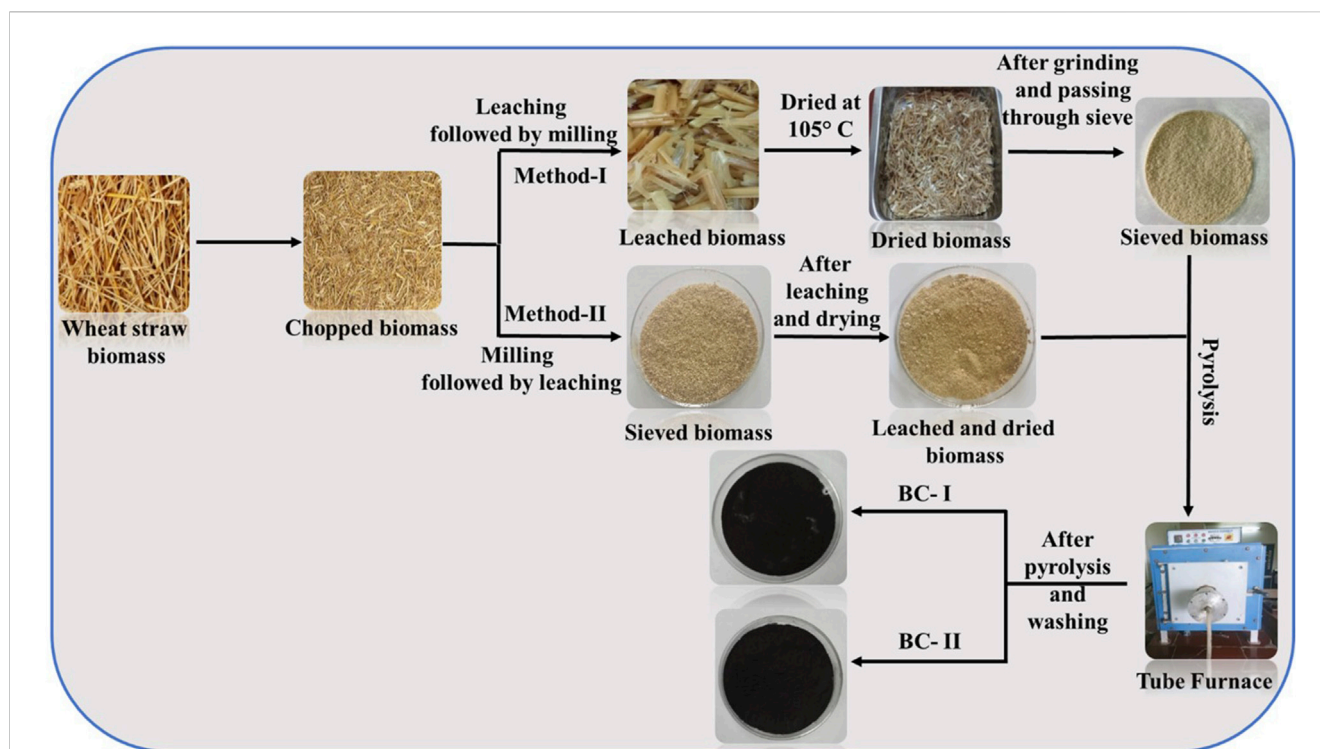


FIGURE 1

Schematic representation for the synthesis of BC-I and BC-II. BC-I originating from Method-I and BC-II deriving from Method-II.

made with deionized water. Without additional purification, analytical-grade chemicals were employed.

2.2 Synthesis of biochar

The synthesis of the wheat straw adsorbent materials was investigated using two methods, illustrated in Figure 1. The first method involved the physical cutting of wheat straw to 1–2 cm pieces. The cut straw was then leached in deionised water (10 g/L) for 24 h at room temperature. The leached wheat straw was then separated using vacuum filtration and dried in Jupiter Engineering Works Hot Air Oven for 24 h at 105°C. The dried wheat straw was milled using a Retsch GM200 Grindomix knife mill and was sieved through a 0.25 mm sieve using a Retsch AS200 Vibratory Sieve Shaker.

The second protocol utilised the cut wheat straw waste in method-I and milled it using a Retsch GM200 Grindomix knife mill, followed by sieving (0.25 mm) using the same vibratory sieve stack mentioned above. This fraction was subsequently leached and separated using vacuum filtration and dried in the same manner as in method-I. The leached wheat straw feedstocks obtained through the two pre-treatment protocols were pyrolyzed in a Jupiter Engineering Works single zone tube furnace under nitrogen (99.99%) at 400°C, 10°C/min, holding for 10 min before cooling to ambient temperature. The resultant carbonised straw was washed with ethanol and acetone to remove bio-oil/tar residues liberated under the pyrolysing environment (until the washings ran from

yellow to colourless), followed by drying at 105°C overnight. The collected samples were designated as BC-I and BC-II.

2.3 Characterization of solid samples

Using a Perkin Elmer FTIR spectrometer, FTIR spectra of samples between 400 cm^{-1} and 4,000 cm^{-1} were obtained. Proximate analysis of the raw wheat straw feedstock was carried out using a LECO 701 thermogravimetric analyzer at ~1.00 g scale where moisture, devolatilization, and ash were measured. Thermogravimetric analysis was carried out as follows: ambient to 107°C at 3°C/min under nitrogen, holding for 15 min (moisture phase) before heating from 107°C to 950°C at 5°C/min, holding for 7 min (volatile phase) before cooling to 600°C. This was followed by an ashing phase in air from 600°C to 750°C at 3°C/min, before cooling to ambient temperature. Fixed carbon was calculated by subtracting the final ash mass from the sample mass before combustion. Ultimate analysis of all feedstocks was acquired using a LECO Truspec CHN Combustion analyzer using sample sizes of 50.00–70.00 mg. Scanning Electron Microscopy (SEM) images were collected via a Zeiss EVO 60 instrument at 10⁻² Pa and an electron acceleration voltage of 20 kV. Powders were adhered to a coated conductive carbon tape and attached to the specimen holder. Available surface area and porosity was measured using a Micrometrics TriStar porosimeter, prior to analysis samples were degassed for 3 h at 110°C under a nitrogen capillary feed.

TABLE 2 BET surface area, pore diameter, and pore volume for BC-I and BC-II.

Sample	BET surface area (m ² /g)	Pore diameter (nm)	Pore volume (cm ³)
BC-I	6.284 ± 0.037	9.961	0.010
BC-II	20.754 ± 0.193	7.783	0.035

2.4 Characterization of liquid samples

On a Thermo scientific UV-Vis spectrophotometer, the concentration of RhB in a solution was measured using the characteristic peak at 554 nm using a 3.5 mL quartz cuvette with a path length of 1 cm, over a course of seven concentrations. [Supplementary Figure S1](#) shows the calibration plot for RhB concentration in a solution via UV detection, presenting a high level of experimental accuracy ($R^2 = 0.99797$). For the case of MB, the concentration of the solution was measured using the characteristic MB peak at 664 nm, over a series of dilution factors resulting in a calibration plot where $R^2 = 0.99874$, [Supplementary Figure S1](#).

2.5 Dye adsorption experiments

Experiments were ran at ambient temperature, where a 100 ppm stock solution of RhB and MB were diluted to different concentrations (5, 7.5, 10, 12.5, 15, and 17.5 ppm) in borosilicate vials (30 mL). The pH of each solution was monitored and adjusted for the following, 2, 4, 6, 8, 10, and 12 using 0.1 M NaOH and 0.1 M HCl using a Metrohm Eco Titrator. To evaluate the dye adsorption by the produced materials (BC-I and BC-II), the colour change of RhB and MB dye solutions were monitored while they were constantly agitated using magnetic stirring at 500 rpm. Aliquots were removed periodically for kinetic studies, the BC-I or BC-II materials were separated via microcentrifugation using an Eppendorf Centrifuge 5,425 at 9,000 rpm for 5 min. After analysis by UV-Vis, the liquid was added back into the reaction along with the separated adsorbent.

To determine the effect of adsorbent dosage, 15 mL of each dye solution was treated with 2, 4, 6, 8, 10, 12, and 14 mg of RhB adsorbent, whereas 2, 3, 5, 6, 7, 9, and 10 mg for MB the same masses were used, stopping at 10 mg as no further benefit was found by using more adsorbent after 6 mg. The initial concentration of each dye was set at 10 ppm where the solution was fixed to the ideal pH = 4 for RhB adsorption, 8 mg of BC-I and BC-II adsorbent were added, and the reaction time range was set from 5 to 1,350 min for BC-I and 5–940 min for BC-II. In contrast, MB was adjusted to optimum pH = 8, 6 mg of adsorbent (BC-I and BC-II) was added, the initial concentration was 10 ppm and the reaction time range was set from 5 to 490 min for BC-I and 5–410 min for BC-II, respectively. Eq. 1 expresses the dye removal rate:

$$\text{Dye removal rate} = \frac{(C_o - C_e)}{C_o} \times 100\% \quad (1)$$

where C_o denotes the initial dye concentration of the solution and C_e denotes the dye concentration of the solution at adsorption equilibrium.

3 Results and discussion

3.1 Feedstock and adsorbent characterization

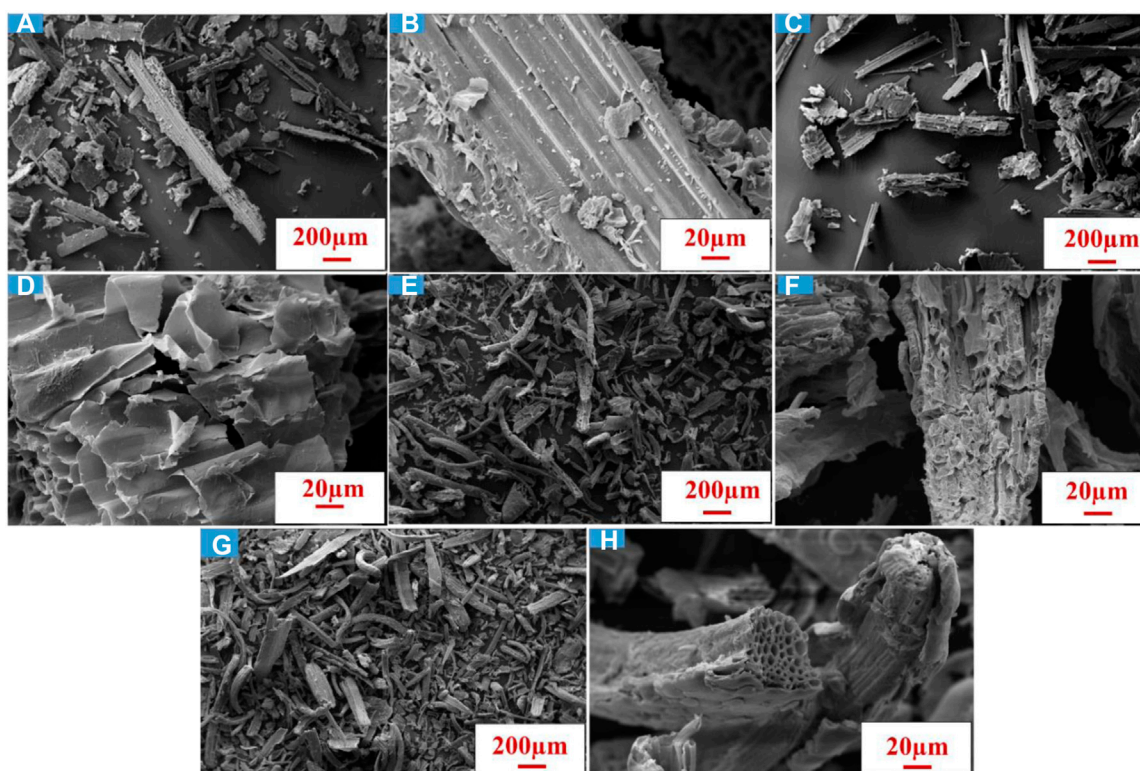
The surface area, pore volumes, and pore diameters of BC-I and BC-II were obtained using the BET (Brunauer-Emmett-Teller) method and the BJH (Barrett-Joyner-Halwnda) method, respectively, as shown in [Supplementary Figure S2](#); [Table 2](#). The isotherm stacked plots shown in [Supplementary Figure S2](#) can be categorized as Type IV. Mesoporous adsorbents exhibit type IV isotherms and feature pores with a size range of 2–50 nm. The surface areas of BC-I and BC-II determined using the BET method were 6.284 m²/g and 20.754 m²/g, respectively. The inset image in [Supplementary Figure S2](#) shows the BJH plots for both BC-I and BC-II, these clearly indicate that pores present are largely below 5 nm, where the average pore sizes shown in [Table 2](#) are 9.96 nm and 7.78 nm for BC-I and BC-II, respectively. This means that the pre-treatment protocol has developed two materials of differing available surface areas and porosities, as BC-II was found to have a pore volume 3.5x higher than BC-I.

[Table 3](#) presents the physical properties of the feedstocks and adsorbent materials. The choice of an effective thermal conversion method is significantly influenced by the moisture content. For a process like a pyrolysis to function properly, the biomass moisture content must not be more than 10%–14% ([Danish et al, 2015](#)). The fact that the unleached and leached samples have a moisture content ranging between 5% and 7% demonstrated the suitability of the raw materials for the manufacture of biochar. The ash content of the wheat straw was found to be naturally higher than other reports ([Arvelakis et al, 2001](#); [Skoglund et al, 2013](#); [Huang et al, 2017](#)). This value was substantially driven down by water washing (leaching), a technique known for the extracting and solubilising water soluble elements such as K, Na, Cl, Mg and to a lesser degree, Ca, S, and Si which often require elevated temperatures for effective removal ([Taylor et al, 2019](#); [Alabdrabalameer et al, 2020](#); [Taylor et al, 2020](#)). [Table 3](#) shows that there is a slightly higher ash value for the second pre-treatment protocol. However, this value could in fact be similar as the first pre-treatment protocol due to a large amount of fixed carbon present in the leached (method-I) sample. The purpose of removing the ash from the wheat straw was to develop the surface area of the material for the pyrolysis step by removing non-carbon entities which could promote or hinder pyrolysis reactions. An example is that alkali metals have been found to previously promote char degradation reactions at high temperatures ([Saddawi et al, 2012](#)). Additionally, metal sites could inhibit the adsorption of dye molecules or in contrast selectively chelate with the organic molecules ([Rana et al., 2018](#)). Unless impregnated directly with a known concentration of such a metal, ash content would act as a rogue entity where adsorption

TABLE 3 Proximate and ultimate analysis of raw and leached feedstocks, as well as biochar samples (BC-I and BC-II).

Samples	Moisture (wt%)	Volatiles (wt%)	Fixed carbon (wt%)	Ash (wt%)	C (wt%)	H (wt%)	N (wt%)	O (wt%) ^a
Raw wheat straw	6.71	81.51	0.17	11.63	39.70	5.21	0.36	43.10
Leached (method-I)	5.23	79.79	10.76	4.22	44.90	6.35	0.07	44.46
Leached (method-II)	6.46	88.45	0.00	5.27	43.30	5.68	0.32	45.43
BC-I	—	—	—	—	51.40	3.27	1.53	43.80
BC-II	—	—	—	—	44.10	1.69	1.21	53.00

^aOxygen is calculated by the summation of ash, C, H and N followed by subtracting from 100.

**FIGURE 2**

SEM micrographs of Wheat straw (A,B) before leaching, (C,D) after leaching (BC-II), (E,F) BC-I after pyrolysis and (G,H) BC-II after pyrolysis.

could not be effectively controlled. Interestingly, the leached (method-I) sample that possessed a high fixed carbon content (Table 3) was also the sample which, after pyrolysis exhibited a diminished surface area and pore volume (Table 2). Table 3 also shows the CHN values of all the materials, after the leaching process there has been an increase in carbon due to a reduction in ash. Interestingly, the carbon value for both leached materials is similar to one and other, where the method-I material has a reduced nitrogen content. Only BC-I shows a mild increase in carbon content from its pre-pyrolyzed counterpart 44.9% and 51.4%, respectively. Whereas the BC-II material has a very similar carbon content to its parent feedstock, 43.3% and 44.1%, respectively. With this in mind, due to the low energy thermal processing method used (400°C), the BC-I and BC-II materials,

although lower in ash still contain a high oxygen content 43.80% and 53.00%, respectively. Typically, higher pyrolysis temperatures are used to remove oxygen from lignocellulosic matter.

The weight loss and derivative weight loss curves (Supplementary Figures S3, S4 respectively) show stacked plots for both the leached materials. Here one can observe the subtle differences between the wheat straw post leaching, using the two protocols. Before carbonization, samples were dried, as a result the samples presented a small weight loss during the moisture phase, illustrated in Table 3. As the temperature increased, there was a sharp weight loss between 215 to 360°C, this is the main volatile region. The greatest mass loss happened at 215–360°C, with a loss of 53.55% and 53.18% for method-I and method-II, respectively as shown in Supplementary Figures S3, S4.

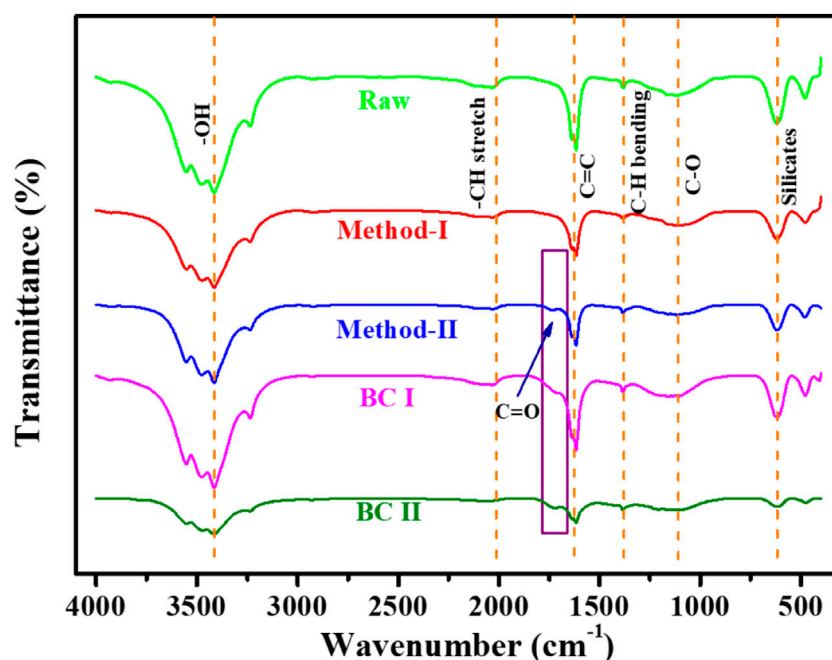


FIGURE 3

Attenuated Total Reflection Fourier transform infrared spectroscopy of Raw, method-I, method-II, BC-I and BC-II.

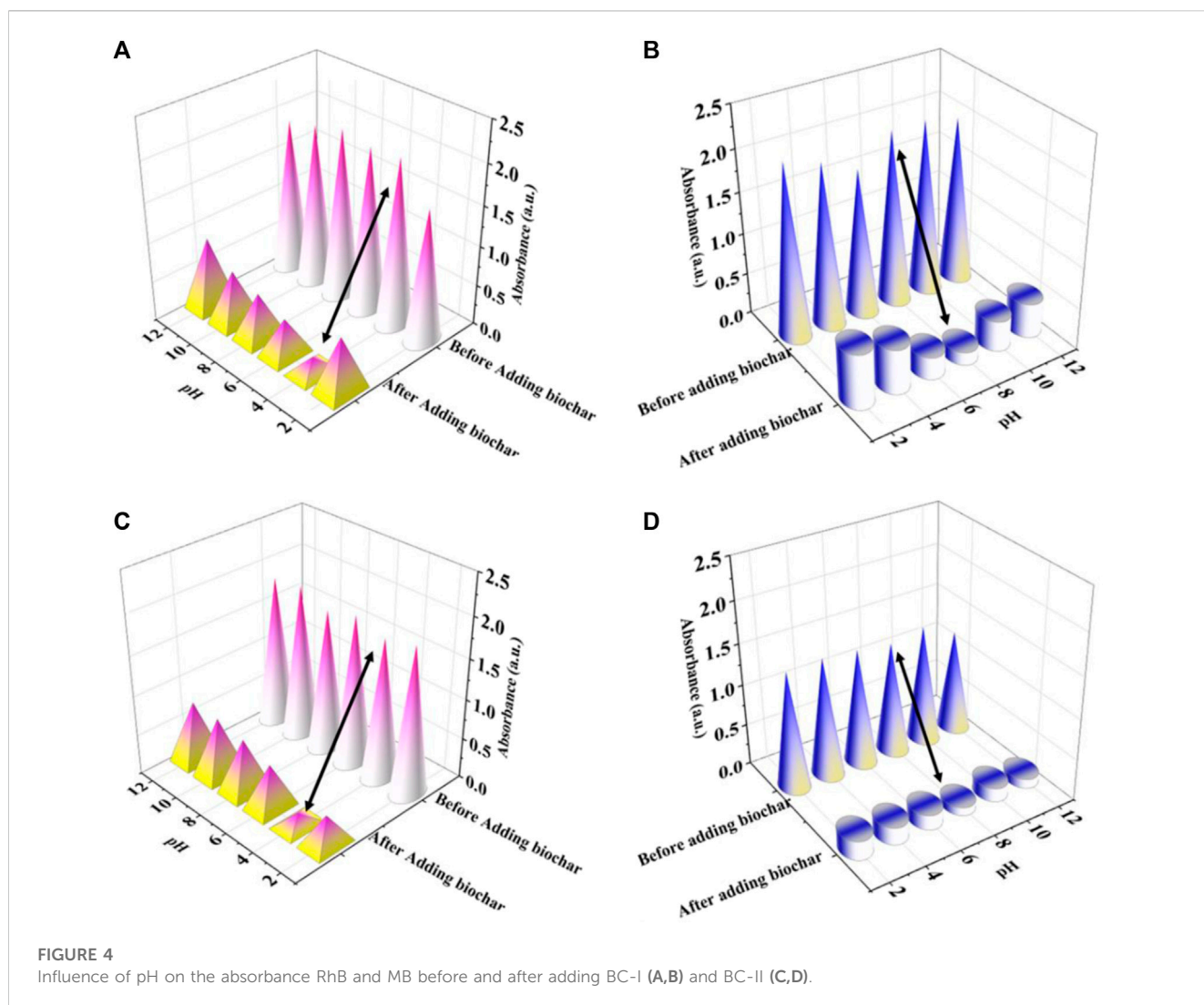
Figure 2 depicts the SEM images of the wheat straw feedstock before leaching, after leaching and after pyrolysis. Electron microscope reveals the surface structure of biochar and gives an elaborate elucidation regarding the dispersion of mesopores in the post pyrolysis materials (Yaashikaa et al, 2020b). The surface topography between the raw and leached wheat straw (Figures 2A, B vs Figures 2C, D, respectively) show that the pre-treatment has caused some mild disruption to the ordered structure by causing some breakages and separation to the wheat straw. Meanwhile, following thermal processing at 400°C, the temperature at which indicated by thermogravimetric analysis that the major volatile components should now be removed. The thermal processing has resulted in a very distorted surface morphology for both BC-I and BC-II, Figures 2E–H, respectively. Figure 2E shows how the ordered structure presented in Figure 2B has been fractured, folded in on itself (Figure 2F) and segments are seen to be separating from the parent grain. Figure 2G also shows the end of a wheat straw grain and its natural pore system (Figure 2H). The temperature used was not high enough to cause dramatic alterations to the ends of the straw sections, instead the low pyrolysis temperature appears to have only impacted the outer surface of the straw, increasing the surface area and porosity of both the carbonised materials, mildly (Supplementary Figure S2; Table 2).

Fourier Transform Infrared Spectroscopy spectra of the raw, leached (method-I), leached (method-II), BC-I and BC-II biomass waste samples are shown in Figure 3. The spectra of the samples disclosed several functional groups that may be in charge of the dye adsorption process. The hydroxy (-OH) stretching vibrations, characteristic of moisture is identified at 3,400 cm^{-1} (Chen and Li, 2020). The peak at 1,616 cm^{-1} are known to be C=C and C=O stretches (Zhao et al, 2021). Both raw and leached materials showed

significant absorbance peaks at 1,382 cm^{-1} , which were identified as C-H bending vibrations (Mupa et al, 2016). At 2033 cm^{-1} , there was additional evidence of C-H stretch. Primary alcohol stretching vibrations, present in the lignin sections of the sample are responsible for the peak at 1,100 cm^{-1} (C-O). The peak at 613 cm^{-1} is characteristic of the silicate minerals (Si-O-Si) found in biochar samples, specifically from the retained ash. Peaks before and after leaching were nearly the same. Method-II material showed an extra peak at about 1730 cm^{-1} , which is identified as lignin and C=O unconjugated hemicellulose stretching vibrations, the latter present due to the low pyrolysis temperature used (Moharm et al, 2022). For BC-I, the O-H group from adsorbed water is still situated at 3,415 cm^{-1} , this region appears more intense than previous samples due to the natural hygroscopic nature of biochars (Chen and Li, 2020). The vibrations of C-O stretching in cellulose and hemicellulose are visible in the band at 1,102 cm^{-1} , again present due to the low pyrolysis temperature used which infers that full devolatilization has not taken place. The stretching vibration of C=C of aromatic components and lignin in the BC-I and BC-II is what created the peak at 1,624 cm^{-1} (Zhu et al, 2014; Li et al, 2016; Janu et al, 2021). The peak of BC-II at 1733 cm^{-1} is also identified as C=O (COOH) vibrations in lignin (El-Sayed, 2011).

3.2 Adsorption studies

A series of dye adsorption tests were performed to assess the viability of carbonized wheat straw materials for wastewater treatment, specifically investigating the effect of solid pre-treatment protocols on the produced material after thermal processing. To mimic real world water ways and treatment



facilities, the adsorbents were continuously stirred into the aqueous RhB and MB solution at room temperature, opposed to a static system. By agitating the suspension, diffusion of the dye molecule into the bio renewable adsorbate as well as diffusion of the material throughout the water sample can be achieved, preventing mass transfer limitations. The mixtures were sampled periodically where after centrifugation (9,000 rpm), the supernatant was utilized to detect the absorbance at a maximum wavelength ($\lambda_{\max} = 554 \text{ nm}$ and 664 nm) to determine the concentrations of RhB and MB dyes, respectively. After analysis, the adsorbate and adsorbent were returned to the stirred mixture.

3.2.1 Influence of pH on adsorption performance

The pH of the solution was found to have a profound effect on the adsorption process. Figure 4 illustrates how pH in the solution affects the removal of RhB and MB. Hence, pH correspondence was studied for RhB and MB solutions between 2 to 12, regulating the acidity of the solution with 0.1 M HCl or 0.1 M NaOH. In the batch studies, dosage amounts of 8 mg of RhB at a concentration of 10 ppm and 6 mg of MB at a concentration of 10 ppm were used to determine the optimum pH value. For RhB, the maximum

removal efficiency was achieved at pH 4, which was 90.44% for BC-I and 91.38% for BC-II. At pH values lower than 4, RhB can be detected as cationic and monomeric molecules. At $\text{pH} > 4$, RhB (Zwitterionic form) in water may cluster to create a larger molecules (dimers), as a result become too large to enter smaller pores in the adsorbent. The attractive electrostatic contact among the carboxyl and xanthene groups of the zwitterionic form (Saddawi et al, 2012; Rana et al., 2018).

For MB, optimal removal efficiency was achieved at pH 8, which was 92.72% for BC-I and 92.52% for BC-II. At low pH, Poor removal arises from the competition between H^+ in the solution and MB^+ , a cationic organic dye present in water. With an increase in pH, the biochar surface starts deprotonated and accumulates negative charges on the surface, which is beneficial for electrostatically absorbing cationic MB dye. The electrostatic contact between deprotonated hydroxyl ($-\text{O}^-$) and deprotonated carboxyl ($-\text{COO}^-$) led to a reduction in adsorption capability in highly alkaline solutions ($\text{pH} > 8$) (Aichour et al, 2018; Thabede et al, 2020), according to a thorough analysis of the aforementioned findings.

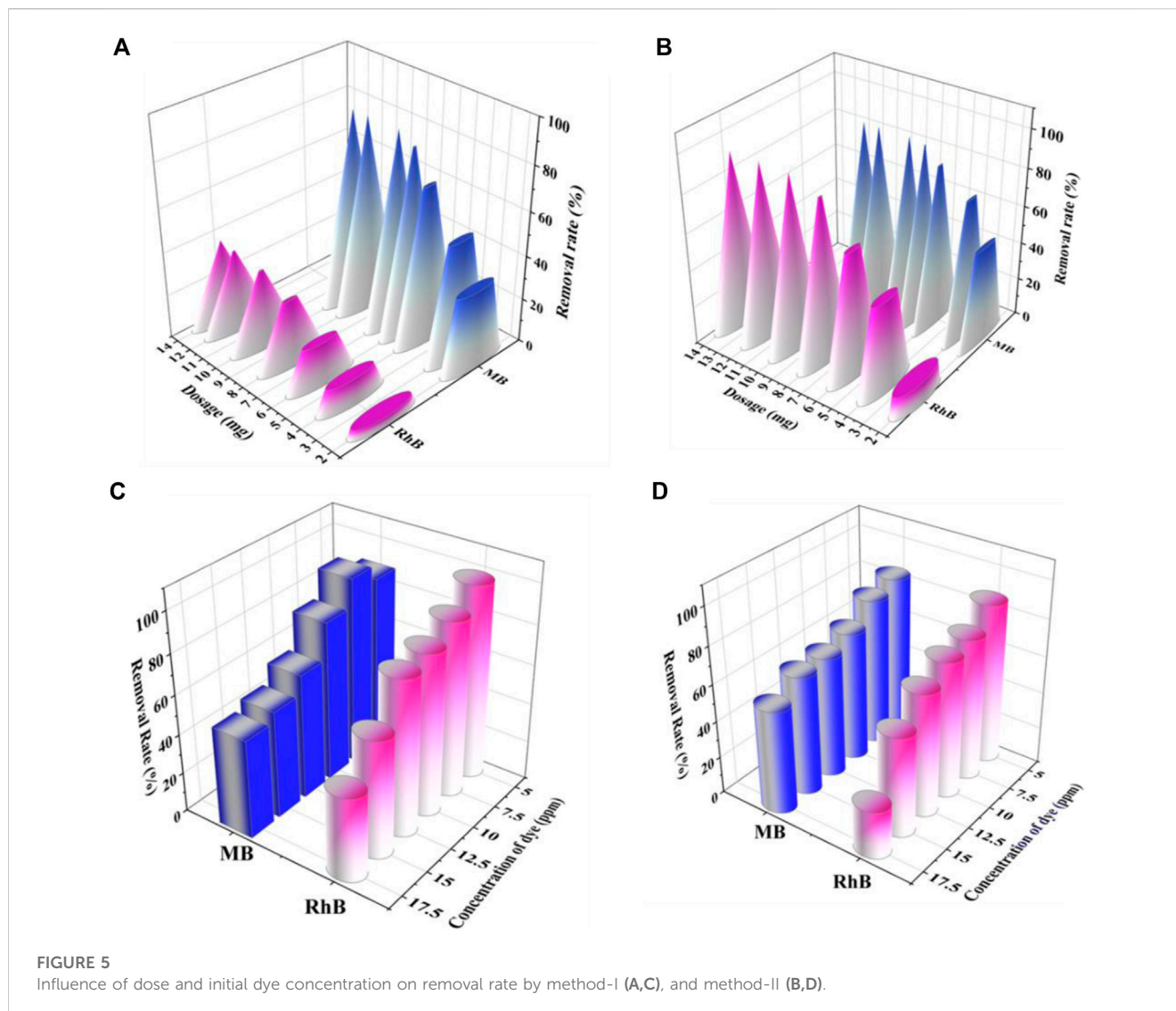


FIGURE 5 Influence of dose and initial dye concentration on removal rate by method-I (A,C), and method-II (B,D).

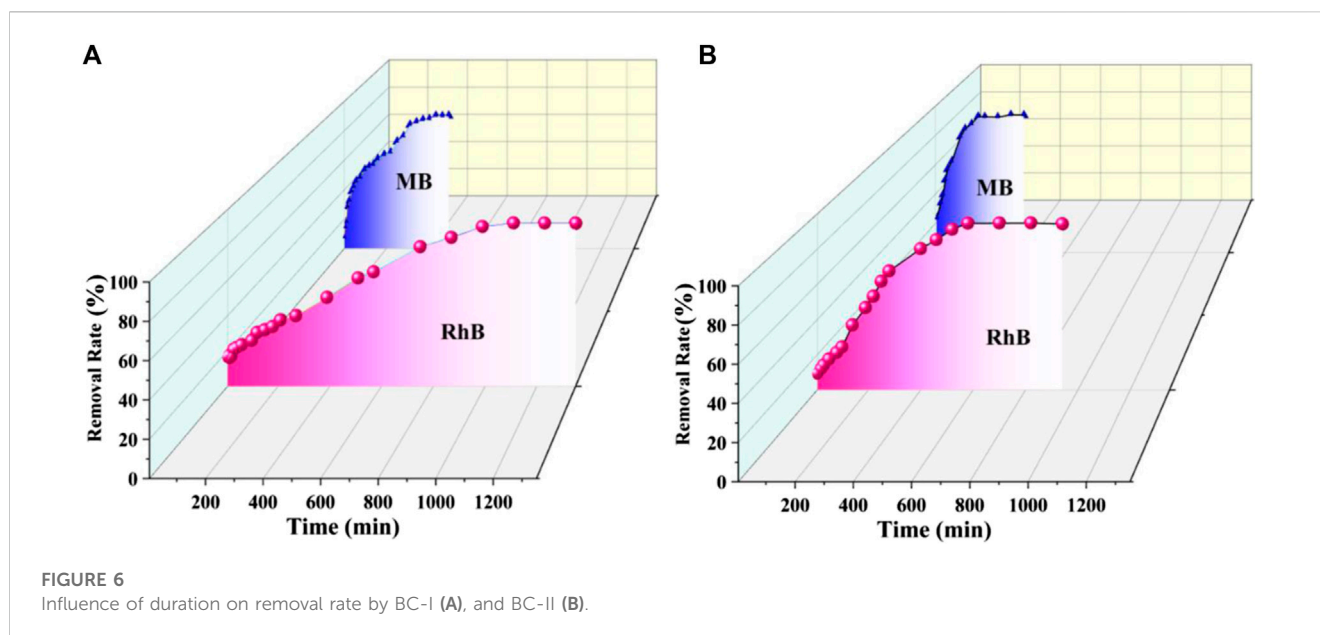
3.2.2 Influence of adsorbent dosage on adsorption performance

Figure 5 exemplifies the impact of biochar dosage on the efficiency of dye removal. The most significant variable influencing the adsorption process is assumed to be the amount of adsorbent present. Insufficient adsorbent dosage can result in poor removal performance, whereas excessive adsorbent might result in ineffective adsorption, leading to inefficient and non-sustainable process. The dosage range trialed was from 2 to 14 mg in 15 mL of RhB solution (10 ppm) at pH 4 (the optimized conditions shown in Figure 4 and from 2 to 10 mg in 15 mL of MB solution (10 ppm) at pH 8. It was shown that increasing the dosage of the adsorbent to 8 mg for RhB dye and 6 mg for MB dye improved the rate of dye removal, for both dyes. This is because as the dosage is increased, a greater number of adsorption sites are made available for the dyes to interact with improving the dye removal rate, without saturating the mixture with idol adsorbent (Gad and El-Sayed, 2009; Gokulan et al, 2019; Sterenzon et al, 2022). This is seen as the dose amount increased, leading to a static adsorption percentage for both dyes (Figures 5A, B).

3.2.3 Influence of initial dye concentration on the adsorption performance

For the batch sorption experiments, BC-I and BC-II were used, with constant adsorbent dosages of 8 mg for RhB and 6 mg for MB. The goal was to examine the dye removal concerning different initial dye concentrations (5, 7.5, 10, 12.5, 15, and 17.5 ppm). According to Figures 5C, D, when dye concentration rises, the rate removal rate falls. At 7.5 ppm for RhB and MB dyes for BC-I, the removal efficiency was observed to be 88% and 94.86%, respectively, however at 17.5 ppm for the same dyes, 42.47% and 50% elimination was observed.

Similarly, for BC-II, the removal effectiveness for RhB and MB dyes was 86% and 84%, respectively at 7.5 ppm, but under comparable circumstances, the dyes concentration of 17.5 ppm demonstrated 25% and 55% elimination. At low concentrations, the adsorbent had adequate active sites. These vacant active sites on the adsorbent were filled with RhB and MB dyes, and saturation of the adsorbent surface was feasible when the dye concentration was increased. This is the reason for the high removal rate at low concentrations. The restricted number of adsorbent surface sites causes saturation (Sara et al, 2016;



Subratti et al, 2021). The removal efficiency will decline when there are more RhB and MB dye species in the solution than there are active sites, this alludes to a rise in dye concentration.

3.2.4 Influence of duration on adsorption performance

Organic molecules in water can diffuse and adhere during the contact duration, which is a critical component in adsorption studies. For RhB dye, 10 ppm solutions regulated to pH 4 was introduced and independently to BC-I and BC-II. The suspensions were mixed as before and the time for maximum dye removal was assessed. Parallel to this, 10 ppm solutions regulated to pH 8 of MB were trialed using the same rate of agitation (500 rpm). For RhB using the optimized extraction conditions, BC-I was found to reach maximum uptake after 900 min (88.00%) whereas the BC-II material, previously shown to have a higher surface area and pore volume (Table 2), reached maximum extraction at 600 min (94.57%), 33% more efficient than BC-I. For the case of MB, Figure 6 shows that removal of this dye is quicker and optimized at higher pH than RhB. When introduced to the carbonized wheat straws BC-I presented maximum extraction at 300 min (94.86%) vs. 170 min for BC-II (92.77%). Once again, BC-II proved to be more efficient as an adsorbate, reaching maximum dye removal in almost half the time as BC-I. Dye extraction profiles are illustrated in Figure 6 where Figure 6A are for BC-I and Figure 6B are for BC-II. The accessibility of more surface adsorption sites for adsorption caused the dye capture rate to increase over time. Dye adsorptive capacity decreased with time due to low dye concentration in the solution and partially or entirely covered adsorption sites of adsorbent (Devi and Saroha, 2017; Cheng et al, 2021).

3.3 Adsorption kinetics

The extraction of RhB and MB were investigated using two alternative kinetic models: pseudo-first-order and pseudo-second-order models. They were assessed for rate constants, adsorption quantity, and correlation coefficient (Vahidhabanu et al, 2019). The

premise of the pseudo-first-order model is that the rate of change in solute adsorption is proportional to the difference between saturation concentration, and the volume of adsorptive material adsorbed over time. According to the Pseudo-second-order kinetic theory, interactions such as ion sharing and transferring among the adsorbent and adsorbate control the adsorption rate. In general, the Pseudo-first-order model demonstrates the presence of physical adsorption and the Pseudo-second-order model demonstrates chemical adsorption.

Pseudo-first-order and pseudo-second-order models were investigated using Eqs 2, 3, respectively, to comprehend the adsorption phenomenon;

$$\log(Q_e - Q_t) = \log Q_e - \frac{K_1 t}{2.303} \quad (2)$$

$$\frac{t}{Q_t} = \frac{1}{K_2 Q_e^2} + \frac{t}{Q_e} \quad (3)$$

where, Q_e and Q_t represent the amount of dye adsorbed (mg/g) at equilibrium and at a time, t (min.), respectively, K_1 and K_2 represent the rate constant for pseudo-first-order (min^{-1}) and pseudo-second-order ($\text{g mg}^{-1} \text{min}^{-1}$) adsorption, respectively (Xiao et al, 2018; Ganguly et al, 2020).

The parameters found by fitting the experimental data to the kinetic Eqs 2, 3 are reported in Table 4 along with the fitting outcomes in Supplementary Figure S5. The correlation coefficient value must be around 1, and the adsorption quantity (Q_e) value must be close to the experimental value, depending on whether the adsorption is well suited for pseudo-first-order or pseudo-second-order (Yaashikaa et al, 2020b). In contrast to the pseudo-first-order equation, which offered excellent fits to the experimental data, the pseudo-second-order model for BC-I and BC-II did not perform well. For the Pseudo-first-order model, the theoretical adsorption quantity is in good accordance with the experimental adsorption quantity for both the dyes by BC-I and BC-II. For BC-I, the correlation coefficient values for the Pseudo first-order model are 0.9545 for RhB and 0.9895 for MB. For BC-II, the correlation coefficient values for the pseudo-first-order model are 0.9989 for

TABLE 4 Pseudo-first-order and pseudo-second-order model variables were fitted to experimental data for the adsorption of RhB and MB dyes onto BC-I and BC-II.

Adsorbent	Dyes	Pseudo-first-order			Pseudo-second-order		
		K_1 (min)	Q_e (mg/g)	R^2	K_2 (g mg ⁻¹ min ⁻¹)	Q_e (mg/g)	R^2
BC-I	RhB	0.0017	9.74	0.9545	0.0016	12.43	0.9984
	MB	0.0143	22.97	0.9895	0.0015	19.53	0.9981
BC-II	RhB	0.0029	13.51	0.9989	0.0011	5.47	0.9912
	MB	0.0219	21.28	0.9933	0.0018	27.12	0.9939

TABLE 5 Variables calculated from Langmuir and Freundlich Isotherm models for the RhB and MB onto BC-I and BC-II.

Adsorbent	Dyes	Experimental Q_M (mg/g)	Langmuir isotherm			Freundlich isotherm		
			Q_M (mg/g)	K_L (L/mg)	R^2	n	K_F (mg ^{1-1/n} L ^{1/n} g ⁻¹)	R^2
BC-I	RhB	19.99	20.40	5.64	0.9789	4.15	16.48	0.9853
	MB	11.05	11.16	2.57	0.9570	2.66	11.99	0.9986
BC-II	RhB	13.87	13.99	17.48	0.9927	2.81	7.29	0.9880
	MB	17.16	17.93	2.17	0.9994	1.15	5.57	0.9932

RhB and 0.9933 for MB. As a consequence, the system adheres to a pseudo-first-order kinetics model with high correlation coefficient values and adsorption quantity for both RhB and MB by BC-I and BC-II. This is due to the physical adsorption that takes place between dyes and the carbonized wheat straw adsorbents in water.

3.4 Adsorption isotherm

An isotherm is a curve that correlates an adsorbate's equilibrium concentration with its capacity to adsorb at room temperature, and it can be used to illustrate how adsorbate and adsorbent interact.

Two isotherm models, including the Langmuir and Freundlich models were experimentally analyzed. The Langmuir adsorption isotherm describes homogenous adsorption which leads to a monolayer covering the adsorbent surface with a limited number of identical sites. The Langmuir equation is represented as follows:

$$\frac{C_e}{Q_e} = \frac{1}{K_L Q_M} + \frac{C_e}{Q_M} \quad (4)$$

Where C_e , Q_e , Q_M , and K_L stand for, in that order, the adsorbate's equilibrium concentrations (mg/L), the ratio of dye adsorbed to adsorbent per gram at equilibrium (mg/g), the highest possible monolayer coverage adsorption capacity (mg/g), and the Langmuir constant (L/mg) (Fan et al, 2016).

The Freundlich adsorption isotherm shows a multilayer coverage because the adsorbates are heterogeneously adsorbing at the surface of the adsorbents. The Freundlich equation is represented as follows:

$$\log Q_e = \log K_F + \frac{1}{n} \log C_e \quad (5)$$

Where C_e , Q_e , and K_F stand for, respectively, the adsorbate's equilibrium concentration (mg/L), the ratio of dye adsorbed to

adsorbent per gram at equilibrium (mg/g), the adsorption intensity, and the Freundlich constant (mg^{1-1/n} L^{1/n} g⁻¹) (El-Hosiny et al, 2018; Maruthapandi et al, 2018).

In addition to the model fits of the isotherm Eqs 4, 5 for RhB and MB by BC-I and BC-II, the parameters derived by employing these equations are shown in Table 5. The R^2 value of the Langmuir and Freundlich model is close to 1 as shown in Table 5. The experimental data matches the Freundlich model more closely than the Langmuir model, as shown by the correlation coefficients (R^2 , Table 5) along with the fitting model as shown in Supplementary Figure S6. These findings disclosed that RhB and MB were adsorbed onto the BC-I and BC-II in a heterogeneous manner, ensuring the multilayer coating of dye molecules on the biochar outer surface. Adsorption is facilitated as values of "n" are greater than unity. The adsorption capacity would be impacted by the carboxyl group because it belongs to the class of functional groups in biochar (Figure 4). The cationic dyes RhB and MB may be adsorbed due to the involvement of the carboxyl group, which has a net negative charge and is possibly the major functional group.

4 FTIR of biochar after dye extraction

Figure 7 displays the ATR-FTIR spectra of BC-I and BC-II on their own as benchmark spectra, followed by the materials after maximum extraction of each dye, using their optimized pH conditions (pH 4 for RhB and pH 8 for MB).

Additionally, the peaks that correspond to the dyes (RhB and MB) will occur when mixing BC-I and BC-II with dye molecules. As a result, peaks were shown to disappear, reappear, and vary. After adsorption, more peaks at 2,935 cm⁻¹ and 2,911 cm⁻¹ were found due to C-H bond stretching in aliphatic formation, demonstrating the presence of RhB and MB dye on the surface of BC-I (Reza et al, 2020). After adsorption, a modest intensity peak for RhB and MB

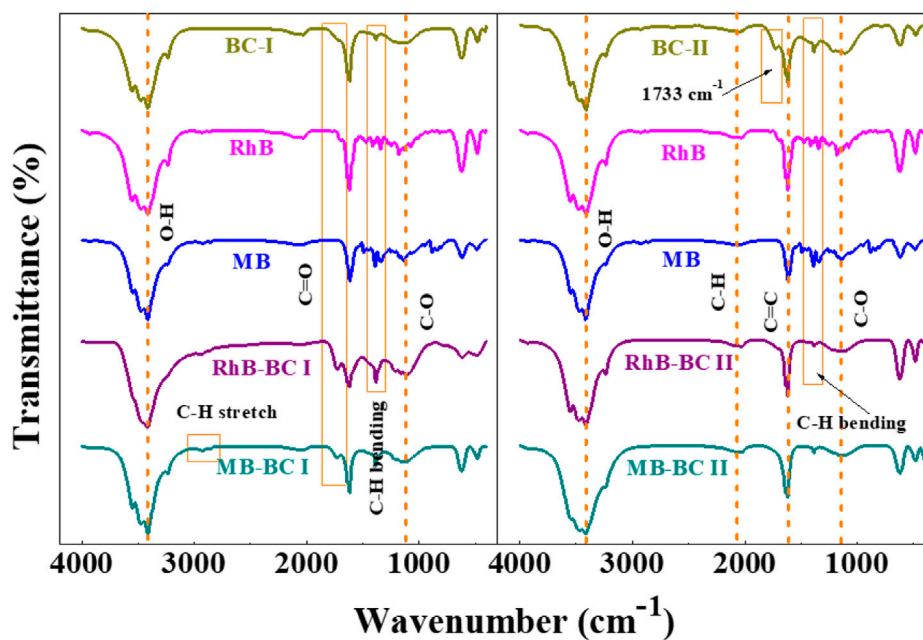


FIGURE 7
FTIR analysis of BC samples, before (A) and after adsorption (B) of both dyes, MB and RhB.

was seen at 1708 cm^{-1} . The signal at 1733 cm^{-1} for BC-II, which was due to C=O group of unconjugated lignin and hemicellulose, disappears after RhB and MB dye have been adsorbed (Moharm et al, 2022).

5 Conclusion

The proposed work puts forward an efficacious synthesis of wheat straw biochar serving as an effective RhB and MB adsorbent. The BC-II synthesized after method-II exhibited better performance as revealed by its adsorption activity towards both dyes, this was corroborated by an increase in available surface area and pore volume. pH studies disclosed that the maximum removal rate was 91.06% for RhB at pH 4% and 92.43% for MB at pH 8. To evaluate the kinetic data, two kinetics models—pseudo-first-order and pseudo-second-order models were employed. The adsorption of dyes onto biochar was deemed to be well averred by pseudo-first-order kinetics, considering the close agreement between theoretical Q_e and experimental Q_e values. It depicts the adsorption intake rate of dyes with $R^2 = 0.9989$ for RhB and $R^2 = 0.9933$ for MB. To evaluate the isotherm data, Langmuir and Freundlich's isotherms were employed and the R^2 value is satisfactory to confidently fit with the Freundlich model. Besides addressing environmental concerns, using wheat straw as the starting base for the creation of an adsorbent offers a sustainable method for creating a viable, reasonably priced adsorbent for the elimination of dye from wastewater. To enhance the adsorption capabilities of biorenewable derived materials, further free and or post processing will need to take place to activate the biochar. Chemical and or physicochemical activation will develop a pore architecture that will increase pore volumes and available surface area.

Data availability statement

The original contributions presented in the study are included in the article/Supplementary Material, further inquiries can be directed to the corresponding authors.

Author contributions

Conceptualization, MT and SM; methodology, Pr; formal analysis, Pr, DV, and MT; investigation, Pr, DV, MT, and SM; resources, SM; supervision, MT and SM; data curation, Pr; writing, review and editing, Pr, DV, MT, and SM. All authors contributed to the article and approved the submitted version.

Funding

Commonwealth research contribution. Commonwealth Scholarship Commission—Split-Site Scholarship 2022 (Ref No. INCN-2022-395).

Acknowledgments

Pr, SM, and MT acknowledge the Commonwealth Scholarship Commission for P's Split-Site Scholarship 2022 (Ref No. INCN-2022-395). P also acknowledges UGC, New Delhi for a Junior Research Fellowship (JRF). Authors are thankful to Sophisticated and Analytical Instrument Facility (SAIF) and the Central Instrumentation Laboratory (CIL) at Panjab University. We would also like to thank Mr. Timothy Dunstan for acquisition of HRSEM images.

Conflict of interest

The authors declare that the research was conducted in the absence of any commercial or financial relationships that could be construed as a potential conflict of interest.

Publisher's note

All claims expressed in this article are solely those of the authors and do not necessarily represent those of their affiliated

organizations, or those of the publisher, the editors and the reviewers. Any product that may be evaluated in this article, or claim that may be made by its manufacturer, is not guaranteed or endorsed by the publisher.

Supplementary material

The Supplementary Material for this article can be found online at: <https://www.frontiersin.org/articles/10.3389/fenvs.2023.1224388/full#supplementary-material>

References

- Adekola, F. A., Ayodele, S. B., and Inyinbor, A. A. (2019). Activated biochar prepared from plaintain peels: Characterization and Rhodamine B adsorption data set. *Chem. Data Collect* 19, 100170. doi:10.1016/j.cdc.2018.11.012
- Ahmed, M. B., Zhou, J. L., Ngo, H. H., Guo, W., and Chen, M. (2016). Progress in the preparation and application of modified biochar for improved contaminant removal from water and wastewater. *Bioresour. Technol.* 214, 836–851. doi:10.1016/j.biortech.2016.05.057
- Aichour, A., Zaghouane-Boudiaf, H., Iborra, C. V., and Polo, M. S. (2018). Bioadsorbent beads prepared from activated biomass/alginate for enhanced removal of cationic dye from water medium: Kinetics, equilibrium and thermodynamic studies. *J. Mol. Liq.* 256, 533–540. doi:10.1016/j.molliq.2018.02.073
- Alabrabalameer, H. A., Taylor, M. J., Kauppinen, J., Soini, T., Pikkarainen, T., and Skoulou, V. (2020). Big problem, little answer: Overcoming bed agglomeration and reactor slugging during the gasification of barley straw under continuous operation. *Sustain Energy Fuels* 4 (7), 3764–3772. doi:10.1039/d0se00155d
- Anfar, Z., Amedlous, A., Ait El Fakir, A., Ait Ahsaine, H., Zbair, M., Lhanafi, S., et al. (2019). Combined methane energy recovery and toxic dye removal by porous carbon derived from anaerobically modified digestate. *ACS Omega* 4 (5), 9434–9445. doi:10.1021/acsomega.9b00524
- Arvelakis, S., Vourliotis, P., Kakaras, E., and Koukios, E. G. (2001). Effect of leaching on the ash behavior of wheat straw and olive residue during fluidized bed combustion. *Biomass Bioenergy* 20, 459–470. doi:10.1016/s0961-9534(01)00003-4
- Chen, J., and Li, S. (2020). Characterization of biofuel production from hydrothermal treatment of hyperaccumulator waste (*Pteris vittata* L) in sub- and supercritical water. *RSC Adv.* 10 (4), 2160–2169. doi:10.1039/c9ra09410e
- Chen, Y., Wang, C., Chen, J., Wang, S., Ju, J., and Kang, W. (2022). Preparing biomass carbon fiber derived from waste rabbit hair as a carrier of TiO₂ for photocatalytic degradation of methylene blue. *Polymers* 14 (8), 1593. doi:10.3390/polym14081593
- Cheng, H., Liu, Y., and Li, X. (2021). Adsorption performance and mechanism of iron-loaded biochar to methyl orange in the presence of Cr⁶⁺ from dye wastewater. *J. Hazard Mater* 415, 125749. doi:10.1016/j.jhazmat.2021.125749
- Chukwu Onu, D., Kamoru Babayemi, A., Chinedu Egbosuba, T., Onyinye Okafor, B., Jacinta Ani, I., Mustapha, S., et al. (2023). Isotherm, kinetics, thermodynamics, recyclability and mechanism of ultrasonic assisted adsorption of methylene blue and lead (II) ions using green synthesized nickel oxide nanoparticles. *Environ. Nanotechnol. Monit. Manag.* 20, 100818. doi:10.1016/j.enmm.2023.100818
- Danish, M., Naqvi, M., Farooq, U., and Naqvi, S. (2015). Characterization of south asian agricultural residues for potential utilization in future 'energy mix. *Energy Procedia.* 75, 2974–2980. doi:10.1016/j.egypro.2015.07.604
- Devi, P., and Saroha, A. K. (2017). Utilization of sludge based adsorbents for the removal of various pollutants: A review. *Sci. Total Environ.* 578, 16–33. doi:10.1016/j.scitotenv.2016.10.220
- Dhanavel, S., Nivethaa, E. A. K., Dhanapal, K., Gupta, V. K., Narayanan, V., and Stephen, A. (2016). α -MoO₃/polyaniline composite for effective scavenging of Rhodamine B, Congo red and textile dye effluent. *RSC Adv.* 6 (34), 28871–28886. doi:10.1039/c6ra02576e
- Egbosuba, T. C., Abdulkareem, A. S., Kovo, A. S., Afolabi, E. A., Tijani, J. O., Auta, M., et al. (2020). Ultrasonic enhanced adsorption of methylene blue onto the optimized surface area of activated carbon: Adsorption isotherm, kinetics and thermodynamics. *Chem. Eng. Res. Des.* 153, 315–336. doi:10.1016/j.cherd.2019.10.016
- El-Hosiny, F. I., Abdel-Khalek, M. A., Selim, K. A., and Osama, I. (2018). Physicochemical study of dye removal using electro-coagulation-floitation process. *Physicochem. Problems Mineral Process.* 54 (2), 321–333. doi:10.5277/ppmp1825
- El-Sayed, G. O. (2011). Removal of methylene blue and crystal violet from aqueous solutions by palm kernel fiber. *Desalination* 272 (1–3), 225–232. doi:10.1016/j.desal.2011.01.025
- Eltaweil, A. S., Abdelfatah, A. M., Hosny, M., and Fawzy, M. (2022). Novel biogenic synthesis of a Ag@biochar nanocomposite as an antimicrobial agent and photocatalyst for methylene blue degradation. *ACS Omega* 7 (9), 8046–8059. doi:10.1021/acsomega.1c07209
- Fan, S., Tang, J., Wang, Y., Li, H., Zhang, H., Tang, J., et al. (2016). Biochar prepared from co-pyrolysis of municipal sewage sludge and tea waste for the adsorption of methylene blue from aqueous solutions: Kinetics, isotherm, thermodynamic and mechanism. *J. Mol. Liq.* 220, 432–441. doi:10.1016/j.molliq.2016.04.107
- Gad, H. M. H., and El-Sayed, A. A. (2009). Activated carbon from agricultural by-products for the removal of Rhodamine-B from aqueous solution. *J. Hazard Mater* 168 (2–3), 1070–1081. doi:10.1016/j.jhazmat.2009.02.155
- Ganguly, P., Sarkhel, R., and Das, P. (2020). Synthesis of pyrolyzed biochar and its application for dye removal: Batch, kinetic and isotherm with linear and non-linear mathematical analysis. *Surf. Interfaces* 20, 100616. doi:10.1016/j.surfin.2020.100616
- Gokulan, R., Avinash, A., Prabhu, G. G., and Jegan, J. (2019). Remediation of remazol dyes by biochar derived from caulerpa scalpelliformis—an eco-friendly approach. *J. Environ. Chem. Eng.* 7 (5), 103297. doi:10.1016/j.jece.2019.103297
- Greenwald, M. J., Redding, A. M., and Cannon, F. S. (2015). A rapid kinetic dye test to predict the adsorption of 2-methylisoborneol onto granular activated carbons and to identify the influence of pore volume distributions. *Water Res.* 68, 784–792. doi:10.1016/j.watres.2014.10.022
- Huang, C., Lai, C., Wu, X., Huang, Y., He, J., Huang, C., et al. (2017). An integrated process to produce bio-ethanol and xylooligosaccharides rich in xylobiose and xylotriose from high ash content waste wheat straw. *Bioresour. Technol.* 241, 228–235. doi:10.1016/j.biortech.2017.05.109
- Janu, R., Mrlik, V., Ribitsch, D., Hofman, J., Sedláček, P., Bielská, L., et al. (2021). Biochar surface functional groups as affected by biomass feedstock, biochar composition and pyrolysis temperature. *Carbon Resour. Convers.* 4, 36–46. doi:10.1016/j.crcon.2021.01.003
- Jury, W. A., and Vaux, H. (2005). The role of science in solving the world's emerging water problems. *Proc. Natl. Acad. Sci.* 102 (44), 15715–15720. doi:10.1073/pnas.0506467102
- Kenchappa Somashekharappa, K., and Lokesh, S. V. (2021). Hydrothermal synthesis of K₂Ti₆O₁₃ nanotubes/nanoparticles: A photodegradation study on methylene blue and rhodamine B dyes. *ACS Omega* 6 (11), 7248–7256. doi:10.1021/acsomega.0c02087
- Kumar, A., Bhattacharya, T., Shaikh, W. A., Chakraborty, S., Owens, G., and Mu, N. (2022). Valorization of fruit waste-based biochar for arsenic removal in soils. *Environ. Res.* 213, 113710. doi:10.1016/j.envres.2022.113710
- Leal Marchena, C., Lerici, L., Renzini, S., Pierella, L., and Pizzio, L. (2016). Synthesis and characterization of a novel tungstosilicic acid immobilized on zeolites catalyst for the photodegradation of methyl orange. *Appl. Catal. B Environ.* 188, 23–30. doi:10.1016/j.apcatb.2016.01.064
- Li, G., Zhu, W., Zhu, L., and Chai, X. (2016). Effect of pyrolytic temperature on the adsorptive removal of p-benzoquinone, tetracycline, and polyvinyl alcohol by the biochars from sugarcane bagasse. *Korean J. Chem. Eng.* 33 (7), 2215–2221. doi:10.1007/s11814-016-0067-9
- Li, X., Wang, S., Duan, L., Hao, J., Li, C., Chen, Y., et al. (2007). Particulate and trace gas emissions from open burning of wheat straw and corn stover in China. *Environ. Sci. Technol.* 41 (17), 6052–6058. doi:10.1021/es0705137
- Li, X., Xu, J., Luo, X., and Shi, J. (2022). Efficient adsorption of dyes from aqueous solution using a novel functionalized magnetic biochar: Synthesis, kinetics, isotherms, adsorption mechanism, and reusability. *Bioresour. Technol.* 360, 127526. doi:10.1016/j.biortech.2022.127526
- Manyà, J. J. (2012). Pyrolysis for biochar purposes: A review to establish current knowledge gaps and research needs. *Environ. Sci. Technol.* 46 (15), 7939–7954. doi:10.1021/es301029g

- Maruthapandi, M., Kumar, V. B., Luong, J. H. T., and Gedanken, A. (2018). Kinetics, isotherm, and thermodynamic studies of methylene blue adsorption on polyaniline and polypyrrole macro-nanoparticles synthesized by C-Dot-Initiated polymerization. *ACS Omega* 3 (7), 7196–7203. doi:10.1021/acsomega.8b00478
- Moharm, A. E., El Naeem, G. A., Soliman, H. M. A., Abd-Elhamid, A. I., El-Bardan, A. A., Kassem, T. S., et al. (2022). Fabrication and characterization of effective biochar biosorbent derived from agricultural waste to remove cationic dyes from wastewater. *Polymers* 14 (13), 2587. doi:10.3390/polym14132587
- Mupa, M., Rutsito, D. D., and Musekiwa, C. (2016). Removal of methylene blue from aqueous solutions using biochar prepared from *Eichhornia crassipes* (Water Hyacinth)-molasses composite: Kinetic and equilibrium studies. *Afr. J. Pure Appl. Chem.* 10 (6), 63–72. doi:10.5897/ajpac2016.0703
- Palansooriya, K. N., Yang, Y., Tsang, Y. F., Sarkar, B., Hou, D., Cao, X., et al. (2020). Occurrence of contaminants in drinking water sources and the potential of biochar for water quality improvement: A review. *Crit. Rev. Environ. Sci. Technol.* 50 (6), 549–611. doi:10.1080/10643389.2019.1629803
- Rana, M., Cho, H. J., Roy, T. K., Mirica, L. M., and Sharma, A. K. (2018). Azo-dyes based small bifunctional metal-organic frameworks for metal chelation and controlling amyloid formation. *Inorganica Chim. Acta* 471, 419–429. doi:10.1016/j.ica.2017.11.029
- Reza, M. S., Afroz, S., Bakar, M. S. A., Saidur, R., Aslftahi, N., Taweekun, J., et al. (2020). Biochar characterization of invasive pennisetum purpureum grass: Effect of pyrolysis temperature. *Biochar* 2 (2), 239–251. doi:10.1007/s42773-020-00048-0
- Rizwan, M., Ali, S., Qayyum, M. F., Ibrahim, M., Zia-ur-Rehman, M., Abbas, T., et al. (2016). Mechanisms of biochar-mediated alleviation of toxicity of trace elements in plants: A critical review. *Environ. Sci. Pollut. Res.* 23 (3), 2230–2248. doi:10.1007/s11356-015-5697-7
- Saddawi, A., Jones, J. M., and Williams, A. (2012). Influence of alkali metals on the kinetics of the thermal decomposition of biomass. *Fuel Process Technol.* 104, 189–197. doi:10.1016/j.fuproc.2012.05.014
- Saghanejad Tehrani, M., and Zare-Dorabei, R. (2016). Highly efficient simultaneous ultrasonic-assisted adsorption of methylene blue and rhodamine B onto metal organic framework MIL-68(Al): Central composite design optimization. *RSC Adv.* 6 (33), 27416–27425. doi:10.1039/c5ra28052d
- Sara, Dawood, Sen, T. K., and Phan, C. (2016). Adsorption removal of methylene blue (MB) dye from aqueous solution by bio-char prepared from *Eucalyptus sheathiana* bark: Kinetic, equilibrium, mechanism, thermodynamic and process design. *Desalination Water Treat.* 57 (59), 28964–28980. doi:10.1080/19443994.2016.1188732
- Singh, S. K. (2016). Progress and performance of agriculture in India. *Econ. Dev. Agric. India* 3 (1), 6.
- Skoglund, N., Grimm, A., Öhman, M., and Boström, D. (2013). Effects on ash chemistry when Co-firing municipal sewage sludge and wheat straw in a fluidized bed: Influence on the ash chemistry by fuel mixing. *Energy Fuels* 27 (10), 5725–5732. doi:10.1021/ef401197q
- Sterenzon, E., Vadiel, V. K., Gerchman, Y., Luxbacher, T., Narayanan, R., and Mamane, H. (2022). Effective removal of acid dye in synthetic and silk dyeing effluent: Isotherm and kinetic studies. *ACS Omega* 7 (1), 118–128. doi:10.1021/acsomega.1c04111
- Subratti, A., Vidal, J. L., Lalgee, L. J., Kerton, F. M., and Jalsa, N. K. (2021). Preparation and characterization of biochar derived from the fruit seed of *Cedrela odorata* L and evaluation of its adsorption capacity with methylene blue. *Sustain Chem. Pharm.* 21, 100421. doi:10.1016/j.scp.2021.100421
- Taylor, M., Alabdrabalemer, H., and Skoulou, V. (2019). Choosing physical, physicochemical and chemical methods of pre-treating lignocellulosic wastes to repurpose into solid fuels. *Sustainability* 11 (13), 3604. doi:10.3390/su11133604
- Taylor, M. J., Alabdrabalemer, H. A., Michopoulos, A. K., Volpe, R., and Skoulou, V. (2020). Augmented leaching pretreatments for forest wood waste and their effect on ash composition and the lignocellulosic network. *ACS Sustain Chem. Eng.* 8 (14), 5674–5682. doi:10.1021/acssuschemeng.0c00351
- Thabede, P. M., Shooto, N. D., and Naidoo, E. B. (2020). Removal of methylene blue dye and lead ions from aqueous solution using activated carbon from black cumin seeds. *South Afr. J. Chem. Eng.* 33, 39–50. doi:10.1016/j.sajce.2020.04.002
- Toledo, P. V. O., Bernardinelli, O. D., Sabadini, E., and Petri, D. F. S. (2020). The states of water in tryptophan grafted hydroxypropyl methylcellulose hydrogels and their effect on the adsorption of methylene blue and rhodamine B. *Carbohydr. Polym.* 248, 116765. doi:10.1016/j.carbpol.2020.116765
- Vahidhabanu, S., Adeogun, A. I., and Babu, B. R. (2019). Biopolymer-Grafted, magnetically tuned halloysite nanotubes as efficient and recyclable spongelike adsorbents for anionic azo dye removal. *ACS Omega* 4 (1), 2425–2436. doi:10.1021/acsomega.8b02960
- Veeramalai, S., Ramlee, N. N., Mahdi, H. I., Manas, N. H. A., Ramli, A. N. M., Illias, R. M., et al. (2022). Development of organic porous material from pineapple waste as a support for enzyme and dye adsorption. *Ind. Crops Prod.* 181, 114823. doi:10.1016/j.indcrop.2022.114823
- Waghchaure, R. H., Adole, V. A., and Jagdale, B. S. (2022). Photocatalytic degradation of methylene blue, rhodamine B, methyl orange and eriochrome black T dyes by modified ZnO nanocatalysts: A concise review. *Inorg. Chem. Commun.* 143, 109764. doi:10.1016/j.inoche.2022.109764
- Wakimoto, R., Kitamura, T., Ito, F., Usami, H., and Moriwaki, H. (2015). Decomposition of methyl orange using C60 fullerene adsorbed on silica gel as a photocatalyst via visible-light induced electron transfer. *Appl. Catal. B Environ.* 166–167, 544–550. doi:10.1016/j.apcatb.2014.12.010
- Wang, P., Wu, C., Guo, Y., and Wang, C. (2016). Experimental and theoretical studies on methylene blue and methyl orange sorption by wheat straw-derived biochar with a large surface area. *Phys. Chem. Chem. Phys.* 18 (43), 30196–30203. doi:10.1039/c6cp04625h
- Wang, P., Yin, Y., Guo, Y., and Wang, C. (2015). Removal of chlorpyrifos from waste water by wheat straw-derived biochar synthesized through oxygen-limited method. *RSC Adv.* 5 (89), 72572–72578. doi:10.1039/c5ra10487d
- xia, Y. J., hai, L. B., Sunmei, X., Jun, Y., and an, C. R. (2009). Adsorption of methylene blue and rhodamine B on baker's yeast and photocatalytic regeneration of the biosorbent. *Biochem. Eng. J.* 45 (2), 145–151. doi:10.1016/j.bej.2009.03.007
- Xiao, Y., Azaiez, J., and Hill, J. M. (2018). Erroneous application of pseudo-second-order adsorption kinetics model: Ignored assumptions and spurious correlations. *Ind. Eng. Chem. Res.* 57 (7), 2705–2709. doi:10.1021/acs.iecr.7b04724
- Xiao, Z., Zhou, J., Fan, L., Li, Y., He, Y., Wang, Y., et al. (2021). Controllable preparation of Cu-MOF-Coated carboxyl filter paper for simultaneous removal of organic dye and metal ions. *Ind. Eng. Chem. Res.* 60 (19), 7311–7319. doi:10.1021/acs.iecr.1c00140
- Yaashikaa, P. R., Kumar, P. S., Varjani, S., and Saravanan, A. (2020a). A critical review on the biochar production techniques, characterization, stability and applications for circular bioeconomy. *Biotechnol. Rep.* 28, e00570. doi:10.1016/j.btre.2020.e00570
- Yaashikaa, P. R., Kumar, P. S., Varjani, S., and Saravanan, A. (2020b). A critical review on the biochar production techniques, characterization, stability and applications for circular bioeconomy. *Biotechnol. Rep.* 28, e00570. doi:10.1016/j.btre.2020.e00570
- Yin, Q., Nie, Y., Han, Y., Wang, R., and Zhao, Z. (2022). Properties and the application of sludge-based biochar in the removal of phosphate and methylene blue from water: Effects of acid treating. *Langmuir* 38 (5), 1833–1844. doi:10.1021/acs.langmuir.1c02946
- Zhang, C., Song, Z., Shi, H., Fu, J., Qiao, Y., and He, C. (2017). The effects of pre-treatments and low-temperature pyrolysis on surface properties of biochar from sunflower straw as adsorption. *Biores.* 12 (1), 1041–1051. doi:10.15376/biores.12.1.1041-1051
- Zhao, F., Shan, R., Li, W., Zhang, Y., Yuan, H., and Chen, Y. (2021). Synthesis, characterization, and dye removal of ZnCl₂-modified biochar derived from pulp and paper sludge. *ACS Omega* 6 (50), 34712–34723. doi:10.1021/acsomega.1c05142
- Zhao, X., Wang, D., Xiang, C., Zhang, F., Liu, L., Zhou, X., et al. (2018). Facile synthesis of boron organic polymers for efficient removal and separation of methylene blue, rhodamine B, and rhodamine 6G. *ACS Sustain Chem. Eng.* 6 (12), 16777–16787. doi:10.1021/acssuschemeng.8b04049
- Zhao, Y., Yang, Q., Yan, B., Liu, B., Gu, Y., Lin, Y., et al. (2022). Aminated polyacrylonitrile nanofiber membranes for the removal of organic dyes. *ACS Appl. Nano Mater* 5 (1), 1131–1140. doi:10.1021/acsnam.1c03759
- Zhu, X., Liu, Y., Zhou, C., Luo, G., Zhang, S., and Chen, J. (2014). A novel porous carbon derived from hydrothermal carbon for efficient adsorption of tetracycline. *Carbon* 77, 627–636. doi:10.1016/j.carbon.2014.05.067